Design and Analysis of a Novel Gravity-Compensating Vertical Linear Motor

BUHYUN SHIN[1] AND KYUNG-MIN LEE[ID][2], (Member, IEEE)
[1]Department of Mechanical Engineering, Hanbat National University, Daejeon 34424, Republic of Korea
[2]School of Mechanical Engineering, Chungnam National University, Daejeon 34134, Republic of Korea

Corresponding author: Kyung-Min Lee (lee.km@cnu.ac.kr)

ABSTRACT We propose a vertical linear motor (VLM) for semiconductor manufacturing equipment that compensates for the weight of the moving part by using the balance of magnetic and elastic forces. The developed VLM achieves zero stiffness with a constant upward force over a working range. The magnetic circuit of the VLM is designed to provide a linear negative stiffness over a ± 2 mm stroke, with an upward force of 14 N at a 0 mm stroke. The negative stiffness is compensated for by the positive stiffness of elastic component-like springs. The upward force is then constant over the working range and corresponds to the weight of the moving part. The proposed VLM is designed to minimize the coupling effects of stiffness and gravity compensation forces by using magnetic flux saturation and magnetic flux path design. We investigate the effects of each design parameter on VLM operation through finite element analysis. Finally, the simulated forces in the proposed VLM are experimentally verified, indicating a linear negative stiffness of approximately -13.5 N/mm and a gravity compensation force of 14.9 N.

I. INTRODUCTION

Gravity compensation is used to study the tradeoff between gravitational energy and other types of energies in order to maintain the total energy during the motion of an object [1], [2]. Gravity compensation can reduce the required capacity of actuators, and consequently, their size, energy consumption, and heat generation. Thus, gravity compensators are often adopted in the rotational joints of robotic systems to ensure the safety of humans and realize energy savings [3]–[5].

Gravity compensation is classified according to the energy source that balances the gravitational energy. A simple solution, known as a counterweight, consists of adding gravitational energy to maintain a constant total gravitational energy [6]–[8]. Although the counterweight is an intuitive solution, it may hamper the system performance due to the increase in mass and volume. Alternatively, a spring and motion transformation mechanism can be used. The spring is an elastic energy source, and the motion transformation

The associate editor coordinating the review of this manuscript and approving it for publication was Engang Tian[ID].

mechanism transmits the gravitational energy of the object to the spring to maintain the sum of the two energy components. Many mechanical components have been used as motion transformation mechanisms, such as wires [9]–[11], gears [12], cams [13], and slide cranks [14]. The magnetic energy provided by a permanent magnet (PM) is also used for gravity compensation. A gravity compensator using magnetic energy was proposed by Boisclair *et al.* [15], but there were difficulties in designing a magnetic circuit that generated sufficient torque to support a heavy robot arm and adjust the nonlinear magnetic force to a torque related to the angular displacement.

A linear gravity compensator for linear motion has different characteristics compared to a rotary gravity compensator. In rotary gravity compensators, the magnitude of the gravity compensation torque depends on the angular displacement of the mass. In contrast, a linear gravity compensator must provide a constant positive upward force, which is a gravity compensation force (GCF), over the working range that is equivalent to the payload on the moving part. However, it can be challenging to achieve zero stiffness over a long stroke. Various studies on zero stiffness in linear motion have been
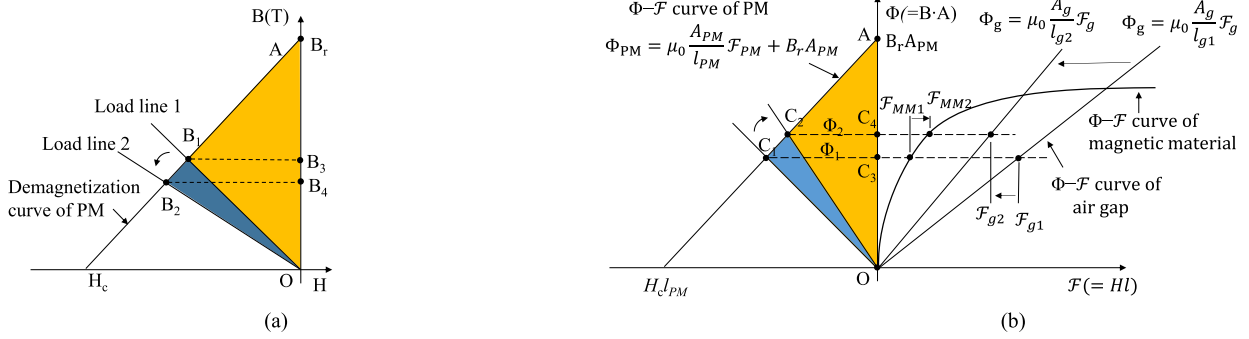
FIGURE 1. (a) Energy per unit volume in PM, and (b) total energy and force generation in magnetic circuits considering PM, magnetic material, and air.

conducted using spring and motion transformation mechanisms [16], [17] or shape memory alloys [18].

As the semiconductor industry pursues ever smaller structures, the corresponding manufacturing equipment requires increasingly high precision. Hence, the dual-stage motion systems consisting of a coarse stage for long strokes and a fine stage for high precision are usually adopted. The fine stage commonly uses linear motors owing to the fast response, no backlash, and simple mechanical structure [19]–[21]. However, a linear motor used for vertical motion in the fine stage should generate sufficient force to support the payload against gravity, consequently generating joule heating, and thereby deteriorating its accuracy. Thus, linear motors that provide gravity compensation have been developed. In [22]–[25], gravity compensation and magnetic levitation were achieved by arranging PMs and balancing their attraction and repulsion forces. In [26]–[29], gravity compensation was achieved by compensating for the magnetic attraction force using the elastic force of elastic members. The linear systems in the semiconductor manufacturing industry use magnetic energy for gravity compensation mainly because of its contactless, noiseless, and frictionless operation. However, it is a challenge to achieve zero stiffness because the stored magnetic energy is nonlinear with respect to the displacement, and it is also affected by factors such as fringing, flux leakage, and saturation of the magnetic material. Additionally, magnetic coupling hinders the decoupling of the stiffness from the GCF and complicates the design of the compensation system. Therefore, it is very challenging to modify any property of a linear gravity compensator.

In this paper, we propose a vertical linear motor (VLM) with a linear negative stiffness and a GCF for gravity compensation. A theoretical analysis of the magnetic energy and force and the conceptual design are described in Section II. The effects of each component on the stiffness, GCF, and linearity of the force profile, are evaluated based on a finite element analysis (FEA) of the detailed VLM design in Section III. The performance of the proposed VLM is verified and compared with the FEA results in Section IV. Finally, the conclusions of this study are presented in Section V.

II. VLM DESIGN
A. MAGNETIC ENERGY IN A GRAVITY COMPENSATOR
The principle of gravity compensation is to maintain the total energy, including the gravitational potential energy. The energy balance in the proposed VLM can be described as

$$\frac{\partial}{\partial z}\left(W_{magnetic} + W_{elastic} + W_{gravity}\right)$$
$$= \frac{\partial W_{magnetic}}{\partial z} + k\Delta z + mg = 0, \quad (1)$$

where $W_{magnetic}$, $W_{elastic}$, and $W_{gravity}$ are the magnetic, elastic, and gravitational energies, respectively, and z, k, m, and g are the vertical displacement, spring constant, mass of the moving object, and acceleration of gravity, respectively. Here, the derivative of the magnetic energy is expressed as a linear equation of the vertical displacement and the weight of the moving object for gravity compensation.

Fig. 1 (a) is a demagnetization curve of a rare earth PM and the area of the orange triangle (OAB_1) corresponds to the magnetic energy per unit volume. The area below segment B_1B_3 corresponds to the energy released to the environment, such as air or a magnetic material [30]–[32]. As the load line moves to B_2, the magnetic energy per unit volume increases to include the area of the blue triangle (OB_1B_2), whereas the force decreases. We modified Fig. 1(a) by multiplying the length and area, and this figure illustrates the total magnetic energy in a system, as shown in Fig. 1(b). The magnetic flux (Φ) – magnetomotive force (MMF, $\mathcal{F}$) curves for a magnetic material and air are added in the first quadrant. In Fig. 1(b), the load line and magnetic flux of the working point are determined by the energy balance between the PM and the air/magnetic material. Specifically, the magnetic flux at the working point is the point at which the magnetic energy (area of triangle OC_1C_3), delivered to the external environment, is equal to the sum of the two areas bounded by $OC_3\mathcal{F}_{g1}$ and $OC_3\mathcal{F}_{MM1}$. Graphically, if the air gap decreases, the $\Phi - \mathcal{F}$ curve of the air gap moves to the left. The MMF on the air gap decreases to $\mathcal{F}_{g2}$ and the magnetic flux and MMF on the magnetic material increases to Φ_2 and $\mathcal{F}_{MM2}$, respectively. As a result, the load line moves upward to point C_2, the

magnetic energy decreases by the area of the blue triangle (OC_1C_2), and the attracting force increases as

$$W_2 - W_1 = \frac{1}{2}B_r\frac{l_{PM}A_{PM}}{\mu_0}\left(B_{PM_2} - B_{PM_1}\right), \qquad (2)$$

$$F = -\frac{\partial W}{\partial l_g} = \frac{1}{2}B_r^2\frac{V_{PM}^2}{\mu_0}A_g$$

$$\times \left(\frac{1}{l_gA_{PM} + A_gl_{PM} + \frac{A_gA_{PM}l_{MM}}{\mu_rA_{MM}}}\right)^2, \qquad (3)$$

where μ_0 and μ_r are the permeability in free space and relative permeability of the magnetic material, respectively. A and l denote the cross-sectional area and length of each material, respectively. The subscripts g and MM indicate the air gap, and magnetic materials, respectively. The values in equation (3), except l_g and μ_r, are constants. μ_r should be varied according to the change in l_g to achieve a linear force profile. The graphical result and equation (3) show that the working point of the PM should be between the linear region and the saturation region to provide a linear negative stiffness while the air gap decreases.

B. CONCEPT DESIGN FOR GRAVITY COMPENSATION

Fig. 2 shows the structure of the proposed VLM (Fig. 2(a)), the integration of multiple VLMs using flexure hinges for gravity compensation (Fig. 2(b)), and the forces on the VLM (Fig. 2(a) and Fig. 2(c)). The VLM delivers a linear negative stiffness and an upward force at the center position, where the stroke is zero. Zero stiffness is achieved by compensating for the negative stiffness with the linear positive stiffness of an elastic component, which corresponds to the flexure hinge in this scenario. In semiconductor manufacturing equipment, four VLMs are located on the four sides of a moving part, and they generate translation along its Z axis and rotations about its X and Y axes. The GCF of each VLM therefore contributes to countering one-quarter of the weight of the moving part, including the wafer being manufactured.

The proposed VLM consists of three PMs—PM$_U$ (above the stator), PM$_D$ (below the stator), and PM$_S$ (on the inner circumference of the stator)—an armature and stator made of ferromagnetic material, and an excitation coil. The armature is composed of two parts: a center disk with a slope, and a flange surrounding the center disk. Both PM$_U$ and PM$_D$ are magnetized symmetrically from the inside to the outside, and they interact with this center disk. The PM$_U$ attracts the armature upward, which is represented as a positive value in Fig. 2(c). The magnitude of the force increases non-linearly as the stroke increases. PM$_D$ attracts the armature downward, which is represented as a negative value, and the magnitude of the force increases non-linearly as the stroke decreases. The two forces are depicted by the blue lines in Fig. 2(c). The symmetrical structure is the reason why the sum of the two non-linear forces results in a linear force profile with a negative stiffness and zero y-intercept, as depicted by black dashed line. The hollow-cylinder PM$_S$ is located at the upper
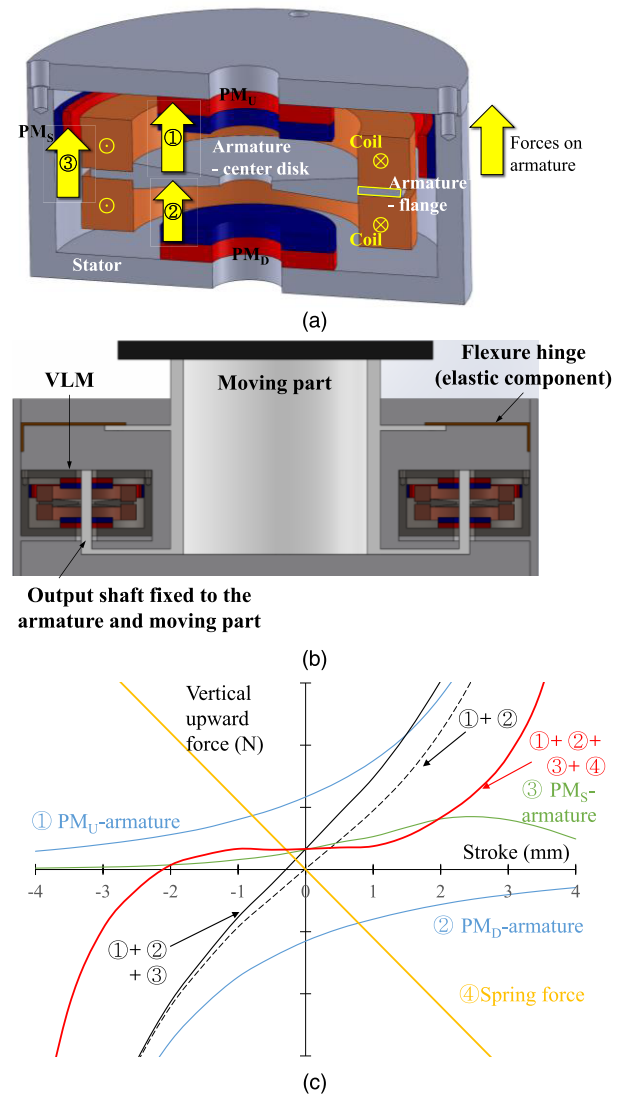

(a)

(b)

(c)

FIGURE 2. Proposed VLM: (a) cross section, (b) cross section of integrated module for gravity compensation, and (c) force components.

side of the inner circumference of the stator. It is magnetized radially from the outside to the inside. The flange is pulled up toward PM$_S$ with a slowly increasing force, which is depicted by the green line, owing to the magnetic flux saturation in the thin flange and the horizontal distance between PM$_S$ and the flange. The sum of the three forces provides a linear negative stiffness and a positive Y-axis intercept for gravity compensation, without excitation, as depicted by the solid black line.

Adding an elastic force with a positive stiffness, depicted by a yellow line in Fig 2(c), helps compensate for the linear negative stiffness, and it achieves a flat force profile as depicted by the red line.

The proposed conceptual design can provide a long stroke with a linear negative stiffness and decouple the magnetic flux governing the stiffness and the GCF. This decoupling allows these two characteristics to be easily adjusted.

III. DETAILED DESIGN

The design requirements corresponded to a semiconductor metrology device with ±2 mm stroke and 14 N GCF. We used the ANSYS Maxwell Axisymmetric 2D model (RZ) to determine the detailed design and analyze the effect of those design parameters on the magnetic force characteristics required for effective gravity compensation. The PM used in the simulation was N48H with 1.4 T of residual magnetization (B_r) and −1061 kA/m coercivity (H_c). The armature and stator material was S45C (medium carbon steel with 0.45% C), which possessed the non-linear BH magnetic property.

The design parameters were selected as shown in Fig. 3. The forces were simulated at stroke intervals of 0.5 mm, as shown in Fig. 4, while the design parameters were varied, as listed in Table 1. Linear regression was applied to the simulated forces over a ±2.5 mm stroke. The slope and upward vertical force at the 0 mm stroke in each linear regression model were treated as the stiffness and GCF, respectively. The simulated force profiles of the developed VLM should be linear to be perfectly compensated by a linear spring constant. Otherwise, the VLM demands additional force control to support the payload. The coefficient of determination R^2 of the linear regression model was used to quantify the linearity of the simulated force profile. This coefficient is a statistical measure of how close the simulated forces are to the linear

regression model. If all the simulated forces are explained by the linear regression model, the value of R^2 is 1. The value decreases as the simulated forces deviate from the linear regression model. In other words, a higher R^2 value indicates that the force profile is more linear. Based on the three indices (stiffness, GCF, and R^2 value), the determined values that satisfied the design requirements were selected, as listed in Table 1. Fig. 5 summarizes the effects of the parameters based on the determined values. For instance, Fig. 5(a) summarizes the eight force profiles in Fig. 4 with the three indexes. As the thickness increases, the stiffnesses increases and the GCFs are almost constant. The value of R^2 reaches a maximum at 2 mm thickness, and the force profile with 2 mm thickness exhibits the most linear force profile over a ±2.5 mm stroke, as shown in Fig. 4.

TABLE 1. Design parameters and variations.

Parts	Design parameter	Evaluated variation	Determined value
Armature	Center disk thickness (average)	0.5 − 4 mm	2 mm (with 5.7° slope)
	Center disk radius	13 − 17.5 mm	13 mm
	Flange thickness	0.5 − 4 mm	1 mm
	Flange length	1 − 6.5 mm	5 mm
PM_U and PM_D	Thickness	2 − 5.5 mm	4 mm
	Radius	8 − 11 mm	10 mm
PM_S	Distance	-2.5 − 4 mm	2 mm
	Length	2 − 6.5 mm	5 mm

A. ARMATURE DESIGN

The ferromagnetic armature was designed to be pulled by the three PMs and achieve the linear negative stiffness characteristics of the proposed VLM. The center disk interacts with PM_U and PM_D and contributes to the stiffness, and the flange interacts with PM_S to contribute to the GCF. Therefore, they should be decoupled.

1) EFFECTS OF CENTER DISK SHAPE

The thickness corresponds to the area of the magnetic material in Fig. 1(b) and is proportional to the magnetic energy capacity. Fig. 6 shows the simulated magnetic fluxes in the armatures for three thicknesses at two different stroke values. For a thin armature of 0.5 mm thickness, the magnetic flux is saturated at a stroke of 0 to 3 mm. The relative permeability is approximately 1 over the stroke range. Thus, the change of magnetic energy in the system is insignificant and the force increment is small, as shown in Fig. 4. For an intermediate-thickness armature of 2 mm, the magnetic flux is not saturated at a stroke of 0 mm, and it is almost saturated at a stroke of 3 mm. The relative permeability decreases over the stroke range, and the linearly increasing force profile

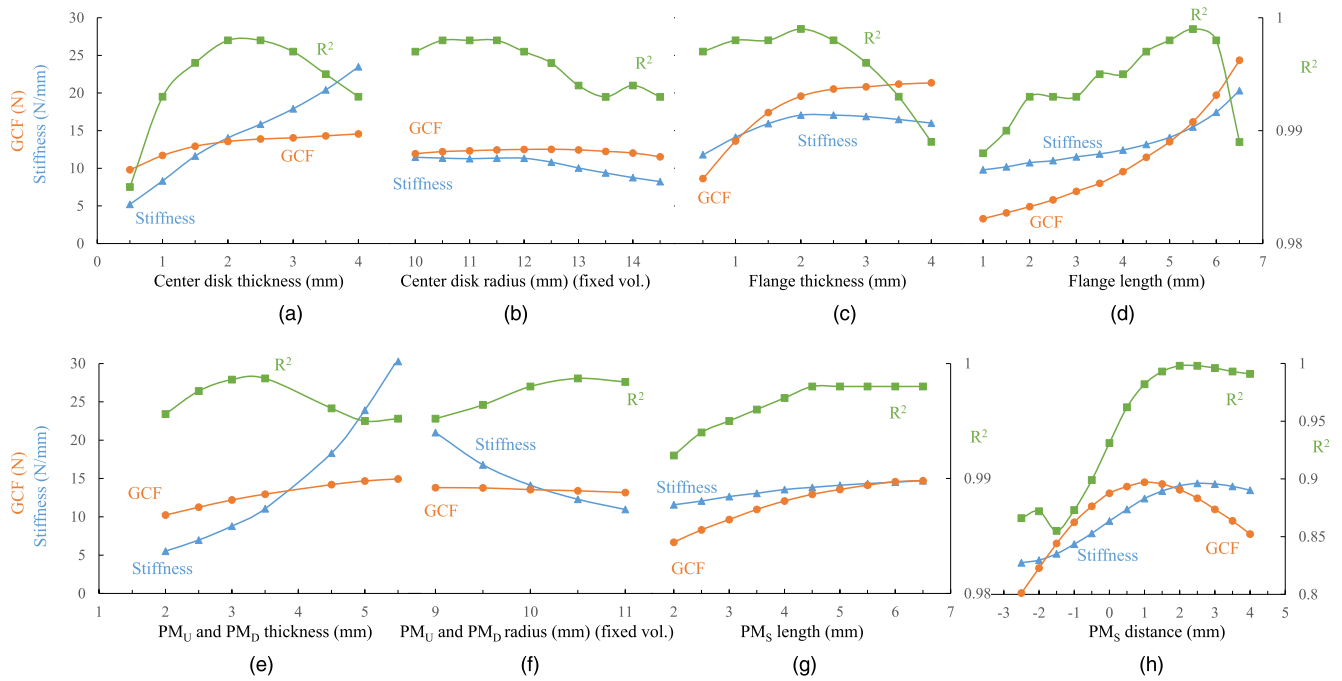**FIGURE 3.** Parameters for the proposed VLM.
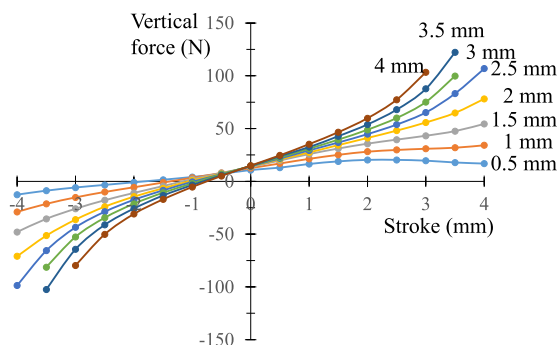
FIGURE 4. Effects of armature thickness on VLM.

FIGURE 5. Effects of design parameters on the three indices.

and the largest R^2 values are exhibited. For a thick armature of 3 mm, the magnetic flux in the armature is not saturated over the stroke range and the force increases nonlinearly. Consequently, this armature exhibits a large stiffness, and the value of R^2 also decreases.

The GCF remains unaffected for thicknesses above 1.5 mm because the magnetic flux in the 1 mm thickness flange, which is flown from the thick center disk, is saturated and the attraction force related to GCF does not change significantly.

Fig. 5(b) shows the effects of the center disk radius on the VLM. To suppress the side effects of the volume and horizontal distance on the three indices, the armature thickness and flange length were decreased while the radius was increased. The volume of the armature is related to the energy capacity, and an increase in volume affects the indices. The center disk radius corresponds to the magnetic path length of the magnetic material shown in Fig. 1(b). A larger radius will horizontally extend the Φ–$\mathcal{F}$ curve of the magnetic material. Nevertheless, this effect can be overlooked because the MMF in the armature was relatively small in the linear region. Moreover, its variation was small compared to the original radius of the center disk. Along with the effect of thickness increase in Fig. 5(a), the results in Fig. 5(b) indicated that the stiffness and GCF were insensitive to the radius. The decrease in the R^2 values with a large radius were due to the non-saturated magnetic flux in the flange, which became thicker than the center disk with decreased thickness.

2) EFFECTS OF FLANGE SHAPE

The flange surrounds the center disk of the armature and interacts with PM_S. Fig. 5(c) shows that the GCF is determined by the flange and PM_S. When the flange was thinner than

the center disk, the linearity of the force profile was high. In contrast, when the flange was thicker than the center disk after 2 mm, the magnetic flux is not saturated in the flange and the force profile became non-linear. Thus, the R^2 value is observed to decrease with a thicker flange.

An increase in the flange length corresponds to an increase in the length of the magnetic material, which is negligible. It also corresponds to a decrease in the horizontal distance between PM_S and armature. Fig. 5(d) shows that a decrease in the horizontal distance contributed to the increase in the GCF, but such a small horizontal distance deteriorates the linearity of the force profile.

In summary, the thickness of the center disk should be designed such that the armature has an intermediate energy capacity and the working point of the magnetic circuit moves from the linear region to the saturation region in the working range to provide high linearity, which was determined to be 2 mm for the proposed VLM. The flange thickness should be designed such that it is saturated in order to keep the upward force constant over the working range and to decouple the GCF from the stiffness. For high linearity, the distance between the PMs and flange should remain above a minimum value, which is determined to be 2 mm for the proposed VLM.

B. PERMANENT MAGNET DESIGN
1) EFFECTS OF PM_U AND PM_D

The PMs are the magnetic energy sources in the VLM. The sizes of the PMs determine the demagnetization curves in the second quadrant and the force profiles. Fig. 5(e) shows the effects of thickness of the PM_U and PM_D on the VLM. The increase in thickness leads to a subsequent
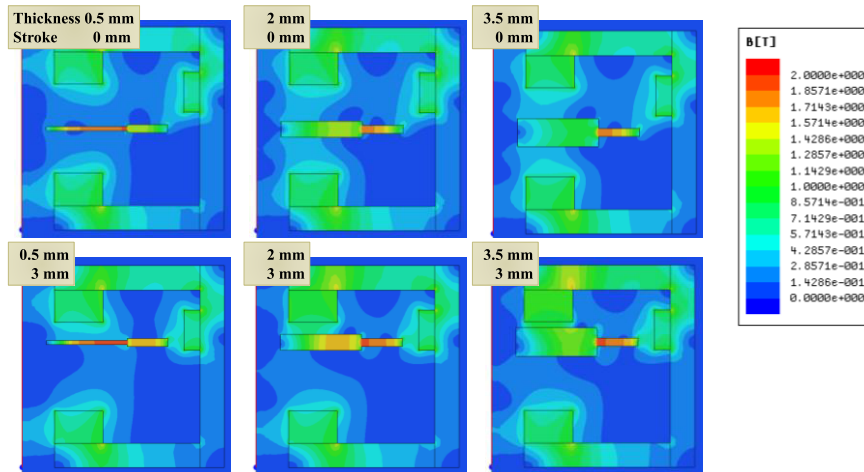
FIGURE 6. Distributions of magnetic field intensity on armatures according to center disk thickness and strokes.

increase in the volume of the PMs and a decrease in the vertical air gap distances between the armature and PM_U and PM_D. Thus, the results in Fig. 5(e) included the side effects of volume increase and the vertical air gap distance decrease. The nonlinear increases in stiffness originated from a combination of an increase in volume and a decrease in the vertical air gap.

Fig. 5(f) shows the effects of the PM_U and PM_D radii for a constant volume and horizontal distance to suppress the side effects of the volume and horizontal distance. It is observed that the GCF was insensitive to PM_U and PM_D, and the R^2 value decreased as the thickness increased.

2) EFFECTS OF PM_S

It was observed that the length of PM_S contributed to the increase in GCF and linearity, as shown in Fig. 5(g). However, the magnetic flux from the top section of a long PM_S circulated on the edge of the stator and did not interact with the armature. Consequently, the length of PM_S did not have a significant effect on the proposed VLM after 4.5 mm.

Fig. 5(h) shows the effect of the location of PM_S. When the bottom of PM_S was vertically coincident with the center of the stator, the distance is reported as 0 mm. When the center of PM_S was vertically located at the center of the stator, the distance is reported as -2.5 mm, and the armature was pulled to the center, compensating for the negative stiffness generated by PM_U and PM_D. As PM_S moved upward, the effect of stiffness compensation decreased, and the GCF and R^2 increased. Once the air gap was sufficiently long and the fringe and leakage increased, the GCF decreased. The stiffness compensation provided by PM_S decreased and only the stiffness by the PM_U and PM_D remained.

In summary, the PM_U and PM_D were related to the stiffness and PM_S was mainly related to the GCF. It was observed that the stiffness was related to the volume of PM_U and PM_D, and the initial air gap was related to the thickness. The GCF was

related to the length of PM_S up to a certain value, which was determined to be 5 mm for the proposed VLM. The location of PM_S may suppress the stiffness due to PM_U and PM_D depending on its location.

IV. EXPERIMENTS AND DISCUSSION

We fabricated and tested the proposed VLM with the determined values in Table 1. The size of the VLM, which provided a stroke of ± 2 mm, was ϕ 50 × 25 mm (diameter × height). The VLM consisted of three neodymium magnets (N48H, Arnold Magnetic Technologies, Rochester, NY, USA) for energy supply, an excitation coil (ϕ 0.3 mm, 720 turns) for position control, and an iron (S45C) armature and stator. The excitation is needed only when the armature moves, because the VLM does not consume electric energy when it is stationary.

During the tests, we measured the magnitude of the negative stiffness and gravity compensation characteristics to compare them with the simulation results of the determined values reported in Section III.

A. LINEAR NEGATIVE STIFFNESS

Fig. 7 shows the experimental setup and its cross-sectional view used to collect the force measurements. The experimental apparatus consisted of the proposed VLM, a load cell (30 Mid, 25 lb, Honeywell, Charlotte, NC, USA), an XYZ-axis manual stage (S3H-12025C, Misumi), and a holding jig. The stator of the VLM was fixed inside the stator holder. The armature and load cell were installed on the stage. The centers of the armature and the stator were aligned using the horizontal axes (X, Y). The stroke of the armature was controlled by the vertical (Z) axis. The upward forces on the armature were measured using the load cell, while the armature was moved up and down at an interval of 0.5 mm over a stroke of ± 2 mm. The net upward forces were calculated
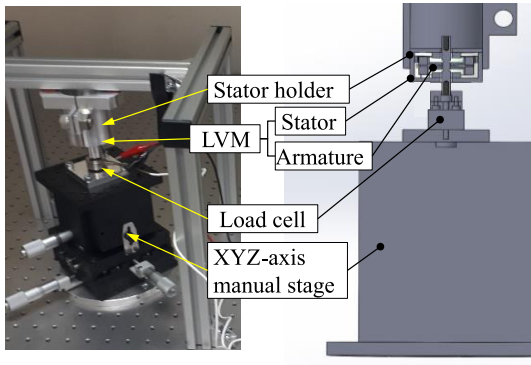
FIGURE 7. Experimental setup for VLM force measurements.
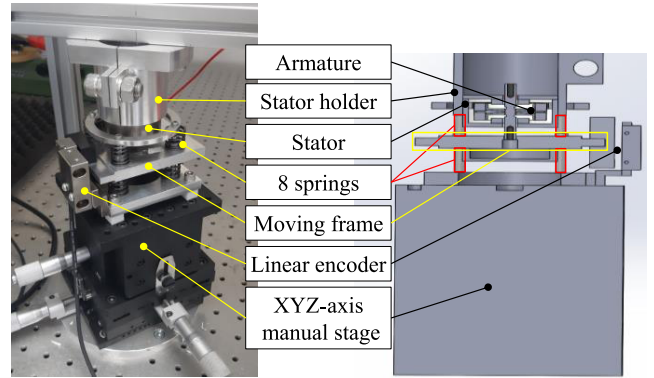

FIGURE 9. Experimental setup for zero-stiffness measurements.

using the measured force by the load cell and the weight of the moving parts connected to the load cell.

Fig. 8 shows the FEA-simulated force, with the determined values in Table 1, and the net upward force. The simulated forces correspond to the solid black line in Fig. 2(c). We simulated two force profiles with the maximum and minimum of the residual magnetization properties as a noise factor, because residual magnetization of the PM used has a range from 1.35 to 1.45. The measured force profile is approximately located between the two simulated force profiles. The measured stiffness and GCF were −13.3 N/mm and 14.9 N, respectively, which were similar to the simulation results.
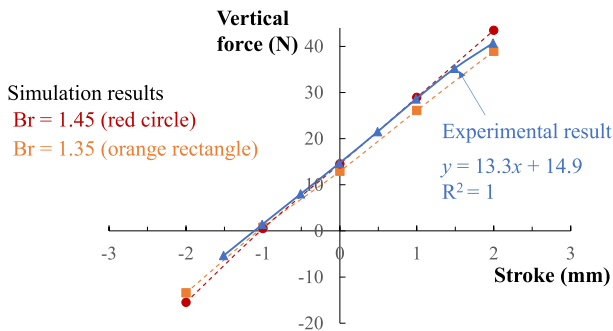

FIGURE 10. Additional force required to achieve equilibrium according to the stroke for a spring constant of 13 N/mm.

exerted by the magnetic energy was larger than the restoring force by 0.8 N/mm with a 13 N/mm spring. The experiment indicated that the stiffness of the VLM was approximately −13.8 N/mm.

C. DISCUSSION

The proposed VLM exhibits stiffnesses of −13.3 and −13.8 N/mm and a GCF of 14.9 N according to the experiments. Table 2 shows the GCF per mass and volume compared to previous gravity compensators. The dimensions of the outer structure were not described in previous research, and only the PM and coils are considered in the mass and volume calculation. However, the stator and armature of the developed VLM are included in the calculations. The developed VLM has a similar force density, even though it includes the structures in the calculation. Additionally, the VLM uses less PM, and the manufacturing cost is much less than the previous gravity compensators.

With regard to the energy consumption, a commercial linear voice coil motor (LVCM-038-038-02, Moticont, 25 N of continuous force) consumes approximates 6.5 W to support 15 N, while the developed VLM consumes no energy. As a result, the developed VLM helps save energy, and also improves the overall performance of the equipment.

FIGURE 8. Generated forces in VLM.

B. ZERO STIFFNESS

To verify the gravity compensation performance of the proposed VLM, we conducted zero stiffness experiments using the experimental setup shown in Fig. 9. The armature was connected to a moving frame by a shaft, which was vertically translating over four ball guides. Eight springs were installed above and below the moving frame corners to generate the restoring forces. The stiffnesses of the springs were set to be slightly different from the VLM stiffness to prevent non-zero stiffness in the resultant force. Thereafter, the upward forces that changed according to the stroke were measured. Fig. 10 shows the forces with 13 N/mm spring stiffness. The slope in the figure represents the difference between the VLM stiffness and the applied spring stiffnesses. The pulling force
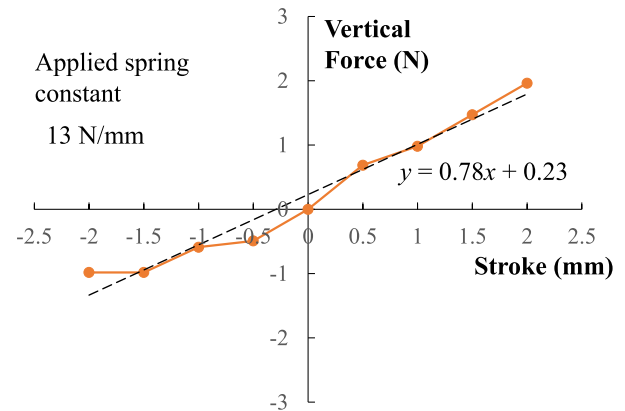
TABLE 2. Comparison of gravity compensation force density.

	GCF (N)	Mass (g)		GCF /Mass (N/kg)	Actuat or Vol. (cm³)	GCF /Vol. (N/cm³)
		PMs /Coils	Struct ure & yoke			
VLM	15	30.0 /64.8	135.3	65.2	49	0.306
[24] (PM& coil)	31	299.2 /157.9	No info.	67.8	154	0.201
[25] (PM& coil)	40	290.3 /54.0	No info.	116	114	0.351

V. CONCLUSION

In this study, we proposed a VLM design that uses the magnetic and elastic forces in the system for gravity compensation. In this design, there is no energy consumption required for supporting the payload against gravity, thus, it saves energy and improves the overall performance of the equipment. A conceptual design for the negative linear stiffness and GCF was first provided based on the total energy in a magnetic circuit considering PM, magnetic material, and air. A detailed design was then performed by analyzing the effects of the VLM parameters on the force profiles using FEA. The FEA results were then experimentally verified, with the proposed VLM exhibiting a GCF of 14. 9 N over ±2 mm according to the experiments. Through the analytical solution, FEA results, and experimental validation, we could establish the following:

1) The working conditions of the magnetic material with a non-linear BH property, such as its linear, transition, and saturation regions, were related to the force profile. In the linear region, the force profile of the magnetic material is proportional to the inverse square of the air gap. The working point of the magnetic material should be moved from a linear region to the transition and saturation regions in order to achieve a linear force profile, as the air gap decreases. Therefore, the thickness of the center disk was determined on the basis of the magnetic energy provided by the PMs and the BH characteristic of the magnetic material to provide high linearity. In addition, the working point of the magnetic material should be designed to be in the saturation region to minimize the variation of force with respect to the stroke. Here, the flange was designed to work in the saturation region in order to achieve a constant upward force.

2) The structure of the proposed VLM decoupled the effects of stiffness and GCF using the magnetic flux saturation in the flange, although there remained slight interactions. The stiffness and GCF can therefore be adjusted independently by adjusting the design parameters of the center disk and the flange, thus providing a more convenient method for modification of the magnetic properties.

3) The thickness or radius alone were insensitive to the stiffness and GCF. The magnitudes of the stiffness and GCF were mainly determined by the air gap distance and volumes of PM and magnetic material, which were related to energy capacities.

The proposed VLM can be applied in semiconductor manufacturing systems, such as a wafer metrology and inspection systems. It can reduce joule heating and energy consumption and improve the accuracy of equipment. Future work will focus on dynamic performance tests and frequency-domain characteristic analyses.

REFERENCES

[1] V. Arakelian, "Gravity compensation in robotics," *Adv. Robot.*, vol. 30, no. 2, pp. 79–96, Jan. 2016, doi: 10.1080/01691864.2015.1090334.

[2] Y. R. Chheta, R. M. Joshi, K. K. Gotewal, and M. ManoahStephen, "A review on passive gravity compensation," in *Proc. Int. Conf. Electron., Commun. Aerosp. Technol. (ICECA)*, Apr. 2017, pp. 184–189, doi: 10.1109/ICECA.2017.8203668.

[3] S. Moubarak, M. T. Pham, R. Moreau, and T. Redarce, "Gravity compensation of an upper extremity exoskeleton," in *Proc. Annu. Int. Conf. IEEE Eng. Med. Biol.*, Aug. 2010, pp. 4489–4493, doi: 10.1109/IEMBS.2010.5626036.

[4] P. W. Hill, E. T. Wolbrecht, and J. C. Perry, "Gravity compensation of an exoskeleton joint using constant-force springs," in *Proc. IEEE 16th Int. Conf. Rehabil. Robot. (ICORR)*, Jun. 2019, pp. 311–316.

[5] R. Altenburger, D. Scherly, and K. S. Stadler, "Design of a passive, iso-elastic upper limb exoskeleton for gravity compensation," *ROBOMECH J.*, vol. 3, no. 1, pp. 1–7, Dec. 2016, doi: 10.1186/s40648-016-0051-5.

[6] G. G. Lowen, F. R. Tepper, and R. S. Berkof, "Balancing of linkages—An update," *Mechanism Mach. Theory*, vol. 18, no. 3, pp. 213–220, 1983, doi:10.1016/0094-114X(83)90092-7.

[7] A. Bayer and G. Merk, "Industrial robot with a weight balancing system," EP Patent 2 301 727 B2, Aug. 24, 2011.

[8] G. C. White and Y. Xu, "An active vertical-direction gravity compensation system," *IEEE Trans. Instrum. Meas.*, vol. 43, no. 6, pp. 786–792, Dec. 1994, doi: 10.1109/19.368066.

[9] D. Lee and T. Seo, "Lightweight multi-DOF manipulator with wire-driven gravity compensation mechanism," *IEEE/ASME Trans. Mechatronics*, vol. 22, no. 3, pp. 1308–1314, Jun. 2017, doi: 10.1109/TMECH.2017.2681102.

[10] C. K. Kim, D. G. Chung, M. Hwang, B. Cheon, H. Kim, J. Kim, and D. S. Kwon, "Three-degrees-of-freedom passive gravity compensation mechanism applicable to robotic arm with remote center of motion for minimally invasive surgery," *IEEE Robot. Automat. Lett.*, vol. 4, no. 4, pp. 3473–3480, Oct. 2019, doi: 10.1109/LRA.2019.2926953.

[11] H.-S. Kim and J.-B. Song, "Low-cost robot arm with 3-DOF counterbalance mechanism," in *Proc. IEEE Int. Conf. Robot. Autom.*, May 2013, pp. 4183–4188, doi: 10.1109/ICRA.2013.6631168.

[12] V. L. Nguyen, C.-Y. Lin, and C.-H. Kuo, "Gravity compensation design of delta parallel robots using gear-spring modules," *Mechanism Mach. Theory*, vol. 154, Dec. 2020, Art. no. 104046, doi: 10.1016/j.mechmachtheory.2020.104046.

[13] K. Koser, "A cam mechanism for gravity-balancing," *Mech. Res. Commun.*, vol. 36, no. 4, pp. 523–530, Jun. 2009, doi: 10.1016/j.mechrescom.2008.12.005.

[14] V. Arakelian and Y. Zhang, "An improved design of gravity compensators based on the inverted slider-crank mechanism," *J. Mech. Robot.*, vol. 11, no. 3, Jun. 2019, Art. no. 034501, doi: 10.1115/1.4043049.

[15] J. Boisclair, P.-L. Richard, T. Laliberte, and C. Gosselin, "Gravity compensation of robotic manipulators using cylindrical Halbach arrays," *IEEE/ASME Trans. Mechatronics*, vol. 22, no. 1, pp. 457–464, Feb. 2017, doi: 10.1109/TMECH.2016.2614386.

[16] C.-C. Lan, S.-A. Yang, and Y.-S. Wu, "Design and experiment of a compact quasi-zero-stiffness isolator capable of a wide range of loads," *J. Sound Vibrat.*, vol. 333, no. 20, pp. 4843–4858, Sep. 2014, doi: 10.1016/j.jsv.2014.05.009.

[17] J. Zhou, X. Wang, D. Xu, and S. Bishop, "Nonlinear dynamic characteristics of a quasi-zero stiffness vibration isolator with cam-roller-spring mechanisms," *J. Sound Vib.*, vol. 346, pp. 53–69, Jun. 2015, doi: 10.1016/j.jsv.2015.02.005.

[18] Y. Araki, K. Kimura, T. Asai, T. Masui, T. Omori, and R. Kainuma, "Integrated mechanical and material design of quasi-zero-stiffness vibration isolator with superelastic Cu–Al–Mn shape memory alloy bars," *J. Sound Vibrat.*, vol. 358, pp. 74–83, Dec. 2015, doi: 10.1016/j.jsv.2015.08.018.

[19] M.-Y. Chen, H.-H. Huang, and S.-K. Hung, "A new design of a submicropositioner utilizing electromagnetic actuators and flexure mechanism," *IEEE Trans. Ind. Electron.*, vol. 57, no. 1, pp. 96–106, Jan. 2010, doi: 10.1109/TIE.2009.2033091.

[20] J.-H. Jeong, M.-H. Kim, S. Woo, D.-G. Gweon, D. Ahn, and D. Hong, "Design of a six-degree-of-freedom motion fine stage driven by voice coil motors with flexural guides," *Int. J. Precis. Eng. Manuf.*, vol. 16, no. 1, pp. 203–207, Jan. 2015, doi: 10.1007/s12541-015-0027-z.

[21] M. Kim, J.-H. Jeong, H. Kim, and D. Gweon, "A six-degree-of-freedom magnetic levitation fine stage for a high-precision and high-acceleration dual-servo stage," *Smart Mater. Struct.*, vol. 24, no. 10, Oct. 2015, Art. no. 105022, doi: 10.1088/0964-1726/24/10/105022.

[22] A. E. Hajjaji and M. Ouladsine, "Modeling and nonlinear control of magnetic levitation systems," *IEEE Trans. Ind. Electron.*, vol. 48, no. 4, pp. 831–838, Aug. 2001, doi: 10.1109/41.937416.

[23] B. Han, Q. Xu, and Q. Yuan, "Multi-objective optimization of a combined radial-axial magnetic bearing for magnetically suspended compressor," *IEEE Trans. Ind. Electron.*, vol. 63, no. 4, pp. 2284–2293, Apr. 2016, doi: 10.1109/TIE.2015.2509905.

[24] H. Zhang, B. Kou, and Y. Zhou, "Analysis and design of a novel magnetic levitation gravity compensator with low passive force variation in a large vertical displacement," *IEEE Trans. Ind. Electron.*, vol. 67, no. 6, pp. 4797–4805, Jun. 2020, doi: 10.1109/TIE.2019.2924858.

[25] H. Zhang, B. Kou, Y. Jin, and H. Zhang, "Modeling and analysis of a new cylindrical magnetic levitation gravity compensator with low stiffness for the 6-DOF fine stage," *IEEE Trans. Ind. Electron.*, vol. 62, no. 6, pp. 3629–3639, Jun. 2015, doi: 10.1109/TIE.2014.2365754.

[26] V. Cardon, "Vertical actuator drive having gravity compensation," U.S. Patent 9 172 291, Oct. 27, 2015.

[27] J. Malaizé, P. Tamigniaux, J. Bordas, and P. Hirsig, "High-accuracy Z actuator relying on a 3-DOF flexural elements-based concept," in *Proc. EUSPEN*, 2018, pp. 1–2.

[28] M. Mittal, V. Tamellini, A. Fasolo, G. Galdos, and S. Szczukiewicz, "Multifunctional Z actuator with an adjustable built-in gravity compensator for high precision systems," in *Proc. 12th Int. Symp. Linear Drives Ind. Appl. (LDIA)*, Jul. 2019, pp. 1–6, doi: 10.1109/LDIA.2019.8771009.

[29] B. Shin, T. Ham, D. Gwak, and K.-M. Lee, "Development of gravity-compensation voice coil motor using negative stiffness," *Trans. Korean Soc. Mech. Eng. A*, vol. 44, no. 8, pp. 597–602, Aug. 2020, doi: 10.3795/ksme-a.2020.44.8.597.

[30] R. P. Deodhar, D. A. Staton, T. M. Jahns, and T. J. E. Miller, "Prediction of cogging torque using the flux-MMF diagram technique," *IEEE Trans. Ind. Appl.*, vol. 32, no. 3, pp. 569–576, May 1996, doi: 10.1109/28.502168.

[31] P. Campbell, "Comments on 'energy stored in permanent magnets,'" *IEEE Trans. Magn.*, vol. 36, no. 1, pp. 401–403, Jan. 2000, doi: 10.1109/20.822554.

[32] P. A. Watterson, "Energy calculation of a permanent magnet system by surface and flux integrals (the flux-mmf method)," *IEEE Trans. Magn.*, vol. 36, no. 2, pp. 470–475, Mar. 2000, doi: 10.1109/20.825815.

BUHYUN SHIN received the B.S. and Ph.D. degrees in mechanical engineering from Seoul National University, Seoul, South Korea, in 2001 and 2007, respectively.

From 2007 to 2009, he worked with Samsung Electronics Company. Since 2012, he has been with the Department of Mechanical Engineering, Hanbat National University, Daejeon, South Korea. His research interests include electromagnetic actuators, mechatronic systems, and biomimetic micromobile robots.

KYUNG-MIN LEE (Member, IEEE) received the B.S. and Ph.D. degrees in mechanical and aerospace engineering from Seoul National University (SNU), Seoul, South Korea, in 2000 and 2006, respectively.

He conducted research at SNU and the University of Toronto, Toronto, ON, Canada, as a Postdoctoral Fellow, and Hyundai Motors Company as a Senior Research Engineer. He was a Patent Examiner with the Korean Intellectual Property Office and an Assistant Professor with Yeungnam University, South Korea. Since 2018, he has been an Assistant Professor with Chungnam National University, South Korea. His research interests include the design, modeling, and control of robot and mechatronic systems.

• • •